EVIDENCE FOR A WIDE RANGE OF UV OBSCURATION IN $Z \sim 2$ DUSTY GALAXIES FROM THE GOODS-*HERSCHEL* SURVEY[*]

Kyle Penner[1], Mark Dickinson[2], Alexandra Pope[3], Arjun Dey[2], Benjamin Magnelli[4], Maurilio Pannella[5], Bruno Altieri[6], Herve Aussel[5], Veronique Buat[7], Shane Bussmann[8], Vassilis Charmandaris[9,10,11], Daniela Coia[6], Emanuele Daddi[5], Helmut Dannerbauer[12], David Elbaz[5], Ho Seong Hwang[8], Jeyhan Kartaltepe[2], Lihwai Lin[13], Georgios Magdis[14], Glenn Morrison[15,16], Paola Popesso[4], Douglas Scott[17], and Ivan Valtchanov[6]

ABSTRACT

Dusty galaxies at $z \sim 2$ span a wide range of relative brightness between rest-frame mid-infrared ($8\,\mu$m) and ultraviolet wavelengths. We attempt to determine the physical mechanism responsible for this diversity. Dust-obscured galaxies (DOGs), which have rest-frame mid-IR to UV flux density ratios $\gtrsim 1000$, might be abnormally bright in the mid-IR, perhaps due to prominent AGN and/or PAH emission, or abnormally faint in the UV. We use far-infrared data from the GOODS-*Herschel* survey to show that most DOGs with 10^{12} L$_\odot$ $\lesssim L_{\rm IR} \lesssim 10^{13}$ L$_\odot$ are not abnormally bright in the mid-IR when compared to other dusty galaxies with similar IR (8–$1000\,\mu$m) luminosities. We observe a relation between the median IR to UV luminosity ratios and the median UV continuum power-law indices for these galaxies, and we find that only 24% have specific star formation rates which indicate the dominance of compact star-forming regions. This circumstantial evidence supports the idea that the UV- and IR-emitting regions in these galaxies are spatially coincident, which implies a connection between the abnormal UV faintness of DOGs and dust obscuration. We conclude that the range in rest-frame mid-IR to UV flux density ratios spanned by dusty galaxies at $z \sim 2$ is due to differing amounts of UV obscuration. Of galaxies with these IR luminosities, DOGs are the most obscured. We attribute differences in UV obscuration to either: 1) differences in the degree of alignment between the spatial distributions of dust and massive stars, or 2) differences in the total dust content.

Subject headings: Galaxies: high-redshift — Infrared: galaxies — Galaxies: ISM

1. INTRODUCTION

At $z \sim 2$, a large fraction of all high mass stars form in dusty galaxies (Chapman et al. 2005; Magnelli et al. 2011). Most of the intrinsic UV emission from newly formed stars in these galaxies is obscured, or absorbed by dust grains that subsequently heat up and radiate at IR wavelengths. The IR luminosity resulting from this obscuration is usually much greater than the emergent UV luminosity. For galaxies in which the intrinsic UV emission from newly formed stars is less obscured, the IR luminosity is still greater than the emergent UV luminosity, but to a lesser degree (Reddy et al. 2012). The relation between the IR and emergent UV emission from a $z \sim 2$ galaxy depends on the interplay between star formation and dust obscuration.

One of the many ways to select dusty galaxies at $z \sim 2$, without redshift determinations from spectroscopy, is to use the ratio of observed 24 to $0.65\,\mu$m (R-band) flux densities (Dey et al. 2008; Fiore et al. 2008). Sources satisfying $S_{24}/S_{0.65} \gtrsim 1000$ have been termed "dust-obscured galaxies", or DOGs; their redshift distribution is approximately a Gaussian that peaks at $z = 2$ with $\sigma_z = 0.5$ (Dey et al. 2008). In the redshift range $1.5 < z < 2.5$, $0.65\,\mu$m observations are sensitive to rest-frame UV emission from newly formed massive stars, and $24\,\mu$m observations are sensitive to mid-IR emission from hot dust and polycyclic aromatic hydrocarbons (PAHs). The DOG criterion is thus unique in that it selects galaxies in a specific redshift range, that also exhibit extreme ratios between their rest-frame mid-IR and UV flux densities. We have yet to understand the physical mechanism driving the span of ratios exhibited by dusty galax-

kpenner@as.arizona.edu

[*] *Herschel* is an ESA space observatory with science instruments provided by European-led Principal Investigator consortia and with important participation from NASA.
[1] Department of Astronomy, University of Arizona, Tucson, AZ 85721
[2] National Optical Astronomy Observatory, Tucson, AZ 85719
[3] Department of Astronomy, University of Massachusetts, Amherst, MA 01003
[4] Max Planck Institut für Extraterrestrische Physik, Postfach 1312, 85741 Garching, Germany
[5] Laboratoire AIM Paris-Saclay, CEA/DSM/Irfu-CNRS – Université Paris Diderot, CEA-Saclay, pt courrier 131, F-91191 Gif-sur-Yvette, France
[6] Herschel Science Center, European Space Astronomy Center, Villanueva de la Cañada, 28691 Madrid, Spain
[7] Laboratoire d'Astrophysique de Marseille, OAMP, Université Aix-marseille, CNRS, 38 rue Frédéric Joliot-Curie, 13388 Marseille cedex 13, France
[8] Harvard-Smithsonian Center for Astrophysics, Cambridge, MA 02138
[9] Department of Physics and Institute of Theoretical & Computational Physics, University of Crete, GR-71003 Heraklion, Greece
[10] IESL/Foundation for Research and Technology – Hellas, GR-71110 Heraklion, Greece
[11] Chercheur Associé, Observatoire de Paris, F-75014 Paris, France
[12] Universität Wien, Institut für Astronomie, Türkenschanzstraße 17, 1180 Vienna, Austria
[13] Institute of Astronomy & Astrophysics, Academia Sinica, Taipei 106, Taiwan
[14] Department of Physics, University of Oxford, Keble Road, Oxford OX1 3RH, UK
[15] Institute for Astronomy, University of Hawaii, Honolulu, HI 96822
[16] Canada-France-Hawaii Telescope, Kamuela, HI 96743
[17] Department of Physics & Astronomy, University of British Columbia, 6224 Agricultural Road, Vancouver, BC V6T 1Z1

ies at $z \sim 2$.

The IR luminosities of DOGs with $L_{IR} \gtrsim 10^{13}$ L$_\odot$ are dominated by emission from active galactic nuclei (AGN; Dey et al. 2008; Bussmann et al. 2009b). The dominant sources of the IR luminosities of less luminous DOGs is a topic of debate. Fiore et al. (2008) and Treister et al. (2009) conclude that the IR luminosities of many DOGs with 10^{12} L$_\odot$ $\lesssim L_{IR} \lesssim 10^{13}$ L$_\odot$ originate from AGN, while Pope et al. (2008) conclude that many such DOGs are powered by newly formed stars.

In this paper, we pose the question "What makes a DOG a DOG?" The primary goal of our study is determining why DOGs have an extreme ratio between their rest-frame mid-IR and UV flux densities when compared to other dusty galaxies. Unfortunately, the simple and singular selection criterion cannot distinguish between a DOG that is:

- abnormally bright at rest-frame 8 μm for its far-IR flux density, indicating its mid-IR luminosity may be dominated by AGN emission, or abnormally strong emission from polycyclic aromatic hydrocarbons (PAHs);

- or, abnormally faint in the rest-frame UV for its optical flux density, indicating that dust more completely obscures the newly formed stars in the galaxy.

We use *Herschel* (Pilbratt et al. 2010) data in the Great Observatories Origins Deep Survey-North (GOODS-N) region (Elbaz et al. 2011) to show that, on average, DOGs with 10^{12} L$_\odot$ $\lesssim L_{IR} \lesssim 10^{13}$ L$_\odot$ are not abnormally bright at 8 μm, but are more UV faint than other galaxies with similar IR luminosities. The ratio between rest-frame IR and UV flux densities is set by the amount of obscuration, which can vary with either: 1) the degree of alignment between the spatial distributions of dust and massive stars, or 2) the total dust content.

This paper is organized as follows. We present the data and sample selection in §2; in §3, we show the results. We discuss the implications of these results in §4, and conclude in §5. We assume a cosmology with $H_0 = 70$ km s^{-1} Mpc $^{-1}$, $\Omega_m = 0.3$, and $\Omega_\Lambda = 0.7$.

2. DATA

2.1. *Measured quantities*

Our study uses observations of the GOODS-N region, which is roughly 10 arcmin × 16.5 arcmin in extent. We cull the sample of DOGs from a catalog of 24 μm sources produced for the *Spitzer*/MIPS survey of the GOODS-N region (M. Dickinson, PI; Magnelli et al. 2011). A 24 μm source is defined as a $\geq 3\sigma$ flux density measurement from PSF fitting to *Spitzer*/IRAC 3.6 μm source priors. The catalog is 99% complete at $S_{24} > 50\,\mu$Jy, and contains 1603 sources.

The 2.2 μm (K_s-band) image we use to identify counterparts for the 24 μm sources comes from observations using the Canada-France-Hawaii Telescope (CFHT). The data are presented in Wang et al. (2010); we use our own reductions (Lin et al. 2012). The 0.65 μm (*R*-band) Subaru image we use to define the DOG sample comes from Capak et al. (2004). The 5σ depth of the 2.2 μm image is $\sim$0.60 μJy (24.5 AB mag); the 3σ depth of the 0.65 μm image is $\sim$0.05 μJy (27.2 AB mag).

To extract flux densities, we follow a modified version of the procedure used by Pope et al. (2008). Using SExtractor (Bertin & Arnouts 1996), we place 3″ diameter apertures at the positions of sources detected ($\geq 5\sigma$) in the 2.2 μm image. If the 2.2 μm flux density is detected with S/N $\geq 5\sigma$ but the 0.65 μm flux density is not detected with S/N $< 3\sigma$, we use a 3σ limit for the latter flux density.

To determine rest-frame UV continuum power-law indices, we extract flux densities at 0.45, 0.55, 0.80, and 0.90 μm (the *B*-, *V*-, *I*-, and *z*-bands) from Subaru images (Capak et al. 2004), using the same procedure. We use the 3.6, 4.5, 5.8, and 8 μm flux densities already associated with the 24 μm sources to determine whether or not their spectral energy distributions (SEDs) at these wavelengths behave as power laws; these flux densities come from a catalog produced for the *Spitzer*/IRAC survey of the GOODS-N region, and will be included in catalogs accompanying the GOODS-*Herschel* public data release.

For the optical/near-IR photometry, we calculate aperture corrections, defined as the ratios of total flux density to flux density in a 3″ diameter aperture for point sources (non-saturated stars). We take the SExtractor parameter `FLUX_AUTO` as the total flux density. The corrections are factors of 1.086, 1.225, 1.247, 1.057, 1.086, and 1.057 at 0.45, 0.55, 0.65, 0.80, 0.90, and 2.2 μm, respectively. To maintain the signal-to-noise ratios given by SExtractor, both the flux densities and their uncertainties are multiplied by these factors.

We associate each 24 μm source with a 2.2 μm source and its extracted optical flux densities if the 2.2 μm source is a unique match within 0.76″ of the position of the 3.6 μm prior. The match radius is chosen by maximizing the number of unique matches while minimizing the number of multiple matches. Of the 1603 24 μm sources, 87 either do not have a $\geq 5\sigma$ 2.2 μm counterpart within the match radius (85 of 87) or have multiple counterparts (2 of 87).

The far-IR flux densities come from a catalog produced for the GOODS-*Herschel* survey (Elbaz et al. 2011). We only use 100 and 160 μm flux densities measured with PACS (Poglitsch et al. 2010), and 250 μm flux densities measured with SPIRE (Griffin et al. 2010), to avoid the complications of measuring flux densities for 24 μm sources in the 350 and 500 μm SPIRE images that are affected by severe source confusion. We consider a $\geq 3\sigma$ measurement at 100 or 160 μm to be a detection; at 250μm, we require a $\geq 5\sigma$ measurement.

We impose additional constraints on the 250 μm flux densities (and 5σ limits), similar to those defining the "clean index" (Hwang et al. 2010; Elbaz et al. 2010, 2011). The 250 μm flux densities of clean sources (and 5σ limits of clean non-detections) should not be affected by severe source confusion. We do not impose additional constraints on the 100 and 160 μm flux densities because the 100 μm images are not deep enough to be affected by source confusion, and the 160 μm images are only deep enough to be moderately affected. The 3σ depths of the 100 and 160 μm images are $\sim$1100 μJy and $\sim$2700 μJy, respectively; the 5σ depth of the 250 μm image is $\sim$5700 μJy.

We attempt to match each 24 μm source to a source with a spectroscopic redshift from the catalogs of

Barger et al. (2008, which includes redshifts compiled from the literature) and Stern et al. (in preparation). We find spectroscopic redshifts for 910 (57%) of the 24 μm sources. If no coincident sources with spectroscopic redshifts are found, we resort to the photometric redshift source catalog of Pannella et al. (in preparation) to find a source match. We exclude sources with photometric redshifts derived from ill-fitting templates (those with reduced $\chi^2 > 2$). For an additional 510 (32%) of the 24 μm sources we have photometric redshift estimates. There are no redshift estimates for 183 (11%) of the 24 μm sources, and these sources are excluded from our samples.

2.2. *Samples*

Using the multi-wavelength information and redshifts, we define 2 samples from the superset of all 24 μm sources with $S_{24} > 50 \, \mu$Jy:

- *DOG sample*: All 24 μm sources with 2.2 μm counterparts and $S_{24}/S_{0.65} > 986$ (Fig. 1). The 24 μm flux density of the faintest DOG is 53 μJy, justifying our $S_{24} > 50 \, \mu$Jy cut for the control sample. The limiting quantity is the depth of the 0.65 μm image ($3\sigma = 0.05 \, \mu$Jy Capak et al. 2004). The redshift distribution of our sample of DOGs is shown in Fig. 2, also motivating our $1.5 < z < 2.5$ cut for the control sample. Six (of 61; 10%) DOGs have spectroscopic redshifts. In the following analysis, we include only DOGs with $1.5 < z < 2.5$. Our conclusions do not change if we include DOGs without redshift estimates in the sample.

- *Control sample*: All $S_{24} > 50 \, \mu$Jy 24 μm sources with 2.2 μm counterparts that are at $1.5 < z < 2.5$, and that do not satisfy the DOG selection criterion. Seventy four (of 268; 28%) control galaxies have spectroscopic redshifts.

For each sample, Table 1 characterizes the subset of sources with flux densities detected at 0.65, 100, 160, and 250 μm. More than 70% of these galaxies are undetected in optical spectra (or are unobserved) because their observed-frame optical flux densities are so faint.

Our sample contains DOGs with fainter 24 μm emission than does the Dey et al. (2008) sample. Their sample is selected from the shallower *Spitzer*/MIPS survey of the Boötes region; their limit is $S_{24} > 300 \, \mu$Jy. However, the GOODS-N region is much smaller than the Boötes region, so we have few DOGs with $S_{24} > 300 \, \mu$Jy. Pope et al. (2008) also study a sample of DOGs in GOODS-N. The main differences between the Pope et al. (2008) sample and ours are that: 1) they limit their sample to $S_{24} > 100 \, \mu$Jy; and 2) they estimate a redshift for each DOG using IRAC and MIPS photometry, whereas we match DOGs to sources in a near-IR/optical catalog, with redshift estimates based on $UBVRIzJK$, 3.6, and 4.5 μm photometry.

The fractions of 24 μm sources at $1.5 < z < 2.5$ that meet the DOG criterion increase with increasing 24 μm flux density (Fig. 1). Of the sources with $S_{24} < 100 \, \mu$Jy, 4% are DOGs. Of the sources with $S_{24} > 100 \, \mu$Jy, 25% are DOGs. Riguccini et al. (2011) find similar fractions; they also find that of their sources with $S_{24} > 300 \, \mu$Jy, 60% are DOGs.
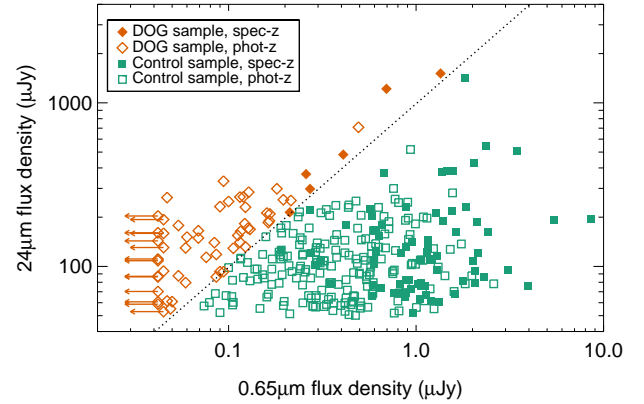

Figure 1. 24 μm flux density vs. 0.65 μm flux density for galaxies in the two samples. The DOG sample is defined by $S_{24}/S_{0.65} > 986$.
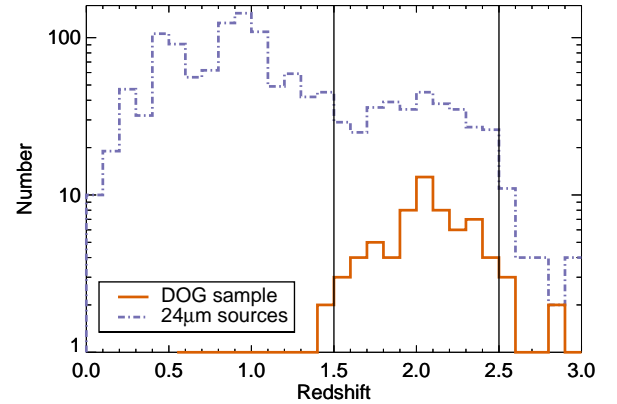

Figure 2. Redshift distributions for the DOG sample and all 24 μm sources (before we impose redshift limits). For the analysis, we limit all samples to the redshift range $1.5 < z < 2.5$ (the area between the vertical lines).

2.3. *Derived quantities*

Several quantities are useful in analyzing the relation between IR and emergent UV emission from galaxies. In this section, we detail how we estimate the total IR and UV luminosities, UV continuum power-law indices, star formation rates, and stellar masses for the galaxies in our samples.

2.3.1. *IR luminosities*

We estimate a total IR luminosity (8–1000 μm; $L_{\rm IR}$) for each galaxy with detected emission at 100 μm. We redshift the Chary & Elbaz (2001) template spectral energy distributions (SEDs) to the distance of each galaxy, find the SED that most closely matches the observed 100 μm flux density, and multiply the IR luminosity of that SED by the ratio between actual and predicted flux densities to get $L_{\rm IR}$.

We prefer this approach over estimating the IR luminosity directly, by summing several far-IR flux densities, because the latter procedure requires detected emission at 160 and 250 μm. The GOODS-*Herschel* image at 160 μm is moderately affected by blending due to source confusion, while the image at 250 μm is so deep that blending is problematic. The drawback to our chosen

Table 1

Sample	Number with $1.5 < z < 2.5$	Median z	Median S_{24} μJy	Number detected			
				$0.65\,\mu$m $\geq 3\sigma$	$100\,\mu$m $\geq 3\sigma$	160μm $\geq 3\sigma$	$250\,\mu$m $\geq 5\sigma$, clean
DOGs	61	2.1	161	47 (77%)	29 (48%)	24 (39%)	9 (15%)
Control	268	2.0	102	268 (100%)	81 (30%)	52 (19%)	15 (6%)

Note. — All sources have $\geq 5\sigma$ $2.2\,\mu$m and $\geq 3\sigma$ $24\,\mu$m flux density measurements. We also require $S_{24} > 50\,\mu$Jy.

approach is that all statements we make regarding IR luminosities assume that the low-redshift template SEDs accurately represent the SEDs of galaxies at $z \sim 2$. Elbaz et al. (2010) show that this assumption is valid when template matching is done to $100\,\mu$m flux densities.

2.3.2. UV continuum power-law indices and luminosities

For galaxies with UV emission from newly formed massive stars, the UV continuum can be approximated as a power law with an index β:

$$S_\lambda = C\lambda^\beta. \tag{1}$$

We use $\geq 3\sigma$ flux densities at 0.45, 0.55, 0.65, 0.80, and $0.90\,\mu$m (i.e., in the B-, V-, R-, I-, and z-bands) to fit for β and the constant factor C for each galaxy which has an estimate of $L_{\rm IR}$. If only two flux densities have S/N $\geq 3\sigma$, we calculate β analytically. If only one flux density has S/N $\geq 3\sigma$, we use an upper limit for the $0.45\,\mu$m flux density to calculate a lower limit to β.

We estimate a UV luminosity λL_λ at rest-frame $0.16\,\mu$m for each galaxy using its redshift estimate and the power-law fit to the rest-frame UV flux densities.

2.3.3. Stellar masses and star formation rates

To estimate a stellar mass for each galaxy, we fit stellar population synthesis models to its $UBVRIzJK$, 3.6, and $4.5\,\mu$m flux densities (Drory et al. 2004; Pannella et al. 2009b). Full details are in §4.2 of Mullaney et al. (2012). We assume the stellar initial mass function in Salpeter (1955) from 0.1 to 100 $M_\odot$, as well as the dust attenuation law in Calzetti et al. (2000).

We use the equation in Kennicutt (1998) to calculate a star formation rate (SFR), based on the IR luminosity, for each galaxy with detected $100\,\mu$m emission. We make no correction for the emergent UV luminosity, since it is negligible for all galaxies in the DOG and control samples (see §4). In using the Kennicutt (1998) equation, we assume that the observed $100\,\mu$m emission is due to star formation and not AGN activity, and that the star formation episode lasts for $< 10^8$ years. Mullaney et al. (2012) find that the former assumption is valid for most AGN with detected X-ray emission at $z < 3$.

3. RESULTS

Seventy six percent of the $z \sim 2$ galaxies with detected $100\,\mu$m emission have 10^{12} L$_\odot$ $\lesssim L_{\rm IR} \lesssim 10^{13}$ L$_\odot$ (Fig. 3). The distributions of IR luminosities for the DOGs and the control galaxies are statistically indistinguishable ($p = 0.20$ that the two samples are drawn from the same parent population, using a K-S test).
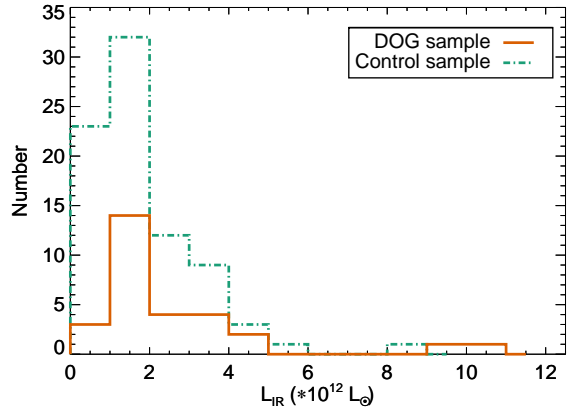

Figure 3. Distributions of IR luminosities (derived from best-fit templates) for galaxies with detected emission at $100\,\mu$m. The two distributions are statistically indistinguishable.
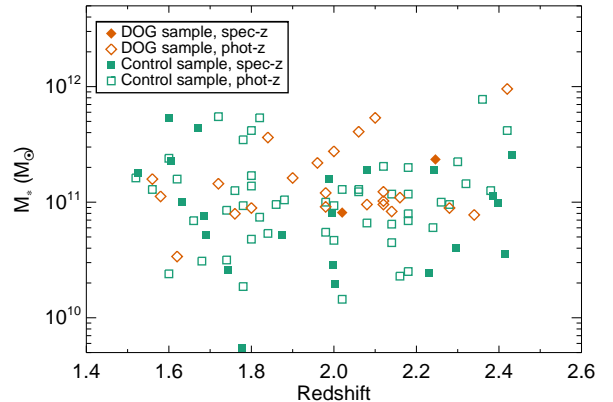

Figure 4. Stellar mass vs. redshift for galaxies with detected emission at $100\,\mu$m. The distribution of stellar masses for DOGs is not strongly different from that for control galaxies, though some control galaxies have lower stellar masses than do the DOGs. Twenty four percent of the control sample has $M_* < 5 \times 10^{10}$M$_\odot$, as opposed to 4% of the DOG sample.

Fig. 4 shows the stellar masses for DOGs and control galaxies with detected emission at $100\,\mu$m. The distributions are not strongly different ($p = 0.02$, using a K-S test), though some control galaxies have lower stellar masses than do the DOGs. 17 (of 72; 24%) control galaxies have stellar masses $M_* < 5 \times 10^{10}$M$_\odot$, while only 1 (of 25; 4%) DOG has a stellar mass below this threshold.

The infrared SEDs of most low redshift dusty galaxies peak between rest-frame ~ 60 and $100\,\mu$m. The rest-frame $8\,\mu$m luminosity is only a fraction of the total IR luminosity in these galaxies. To address whether or not
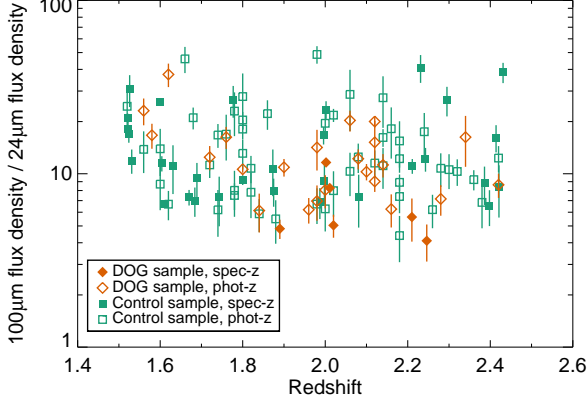
Figure 5. S_{100}/S_{24} vs. redshift for galaxies in the two samples. Galaxies with limits at $100\,\mu m$ are not shown in this figure, but we do include them in our statistical tests. DOGs are statistically indistinguishable from the control galaxies in S_{100}/S_{24}.

Figure 6. S_{250}/S_{24} vs. redshift for galaxies in the two samples. Galaxies with limits at $250\,\mu m$ are not shown in this figure, but we do include them in our statistical tests. As in Fig. 5, DOGs span the same range of flux density ratios as do the control galaxies; this leads us to conclude that the DOG criterion does not select dusty galaxies that are abnormally bright at rest-frame $8\,\mu m$.

DOGs are abnormally bright at rest-frame $8\,\mu m$, we require a comparison of the rest-frame far-IR and $8\,\mu m$ flux densities between DOGs and the control galaxies.

Fig. 5 shows that DOGs are statistically indistinguishable from the control galaxies when looking at the observed flux density ratio S_{100}/S_{24} ($p = 0.35$, using a K-S test) . In this figure, we do not show the galaxies with limits for S_{100}. We perform the Gehan and logrank tests, which are conceptually similar to the two sample K-S test, but also allow for the inclusion of galaxies with limits at $100\,\mu m$ in the two samples. We find no statistically significant difference between the DOGs and the control galaxies ($p > 0.70$ that both samples are drawn from the same parent population, from both tests). Our conclusions are the same using S_{160}/S_{24} (not shown; $p > 0.10$ from both tests). If DOGs were abnormally luminous at rest-frame $8\,\mu m$ for their far-IR luminosities, then we would expect them to have low values of observed S_{100}/S_{24} and/or S_{160}/S_{24} compared to those of the control galaxies; they do not. However, 100 and $160\,\mu m$ observations are sensitive to rest-frame 33 and $53\,\mu m$ emission from galaxies at $z = 2$. These rest-frame wavelengths are still short of the presumed wavelength of the peak of the infrared SED; the rest-frame luminosities are still only a fraction of the total IR luminosity in these galaxies.

$250\,\mu m$ observations are sensitive to rest-frame $83\,\mu m$ emission from galaxies at $z = 2$. This rest-frame wavelength is generally close to the wavelength of the peak of the IR SED. Fig. 6 shows that DOGs are statistically indistinguishable from the control galaxies when looking at the observed flux density ratio S_{250}/S_{24}. We reach the same conclusion when including galaxies with limits at $250\,\mu m$ in statistical tests ($p > 0.76$ that both samples are drawn from the same parent population, from both a Gehan and logrank test).

The DOG criterion does not select galaxies that are abnormally bright at rest-frame $8\,\mu m$ for their far-IR flux densities. What makes a DOG a DOG must be that the galaxy's rest-frame UV emission is suppressed, compared to the UV emission from a control galaxy. Therefore we expect a clear separation between DOGs and control galaxies when looking at the ratios of rest-frame optical to UV flux densities. Indeed, Fig. 7 shows
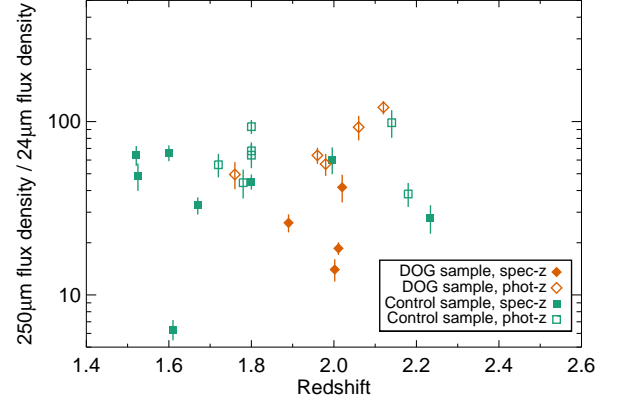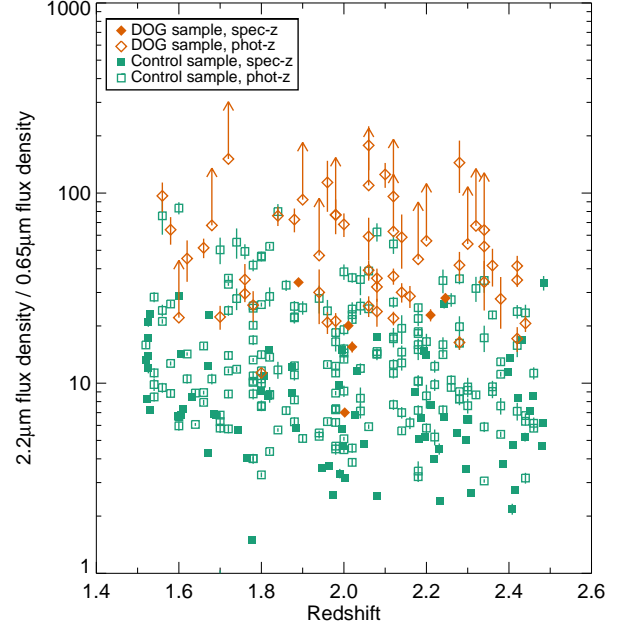

Figure 7. $S_{2.2}/S_{0.65}$ vs. redshift for galaxies in the two samples. A DOG is distinguishable from a random galaxy with detected $24\,\mu m$ emission because it is abnormally faint in the rest-frame UV.

that 92% of DOGs have an observed $S_{2.2}/S_{0.65} > 20$, while 78% of control galaxies have $S_{2.2}/S_{0.65} \lesssim 20$. The Gehan and logrank tests report a statistical difference between the DOGs and control galaxies ($p < 0.0001$ that both samples are drawn from the same parent population, from both tests). Galaxies with $S_{2.2}/S_{0.65} \gtrsim 20$ are also known as "extremely red objects", or EROs (Elston et al. 1988; Hu & Ridgway 1994; Graham & Dey 1996; McCarthy 2004). We note that even though a galaxy with detected $24\,\mu m$ emission may meet the ERO criterion, it may not meet the DOG criterion (and vice versa, rarely).

The statistical difference between the DOGs and con-

trol galaxies for $S_{2.2}/S_{0.65}$, and the lack thereof for S_{100}/S_{24}, is robust against photometric redshift errors. We offset photometric redshifts for the superset of all galaxies with detected $24\,\mu$m emission, assuming the offsets obey a Gaussian distribution with $\sigma_{\Delta z/(1+z)} = 0.1$. We then select new DOG and control samples. The differences in $S_{2.2}/S_{0.65}$ are always statistically significant, and the differences in S_{100}/S_{24} are very rarely statistically significant (from K-S tests).

4. DISCUSSION

We have shown that the 100, 160, and 250 to $24\,\mu$m flux density ratios for DOGs with moderate IR luminosities (10^{12} L$_\odot$ $< L_{IR} < 10^{13}$ L$_\odot$) are statistically indistinguishable from those flux density ratios for galaxies with detected $24\,\mu$m emission that lie at similar redshifts and have similar IR luminosities, but that do not meet the DOG selection criterion. Most DOGs have higher 2.2 to $0.65\,\mu$m flux density ratios than do the control galaxies. Thus it seems clear that DOGs occupy the tail of a distribution of UV obscuration in IR-luminous galaxies at $z \sim 2$.

We select a sample of DOGs using deep images of the GOODS-N region. These DOGs have lower IR luminosities than do DOGs selected using shallower images of wider regions. For example, the Dey et al. (2008) sample in the wide Boötes region contains many DOGs with $L_{IR} > 10^{13}$ L$_\odot$. Our sample contains very few galaxies with $L_{IR} > 10^{13}$ L$_\odot$, and our conclusions regarding obscuration may not apply to DOGs with such high luminosities. At low redshift, AGN emission dominates the IR luminosity for most galaxies with $L_{IR} > 10^{13}$ L$_\odot$ (Tran et al. 2001). Dey et al. (2008) find that many DOGs at $z \sim 2$ with $L_{IR} > 10^{13}$ L$_\odot$ have featureless SEDs from observed-frame 3.6 to $8\,\mu$m, indicating the presence of AGN-heated dust. Several studies (Tyler et al. 2009; Bussmann et al. 2009b; Melbourne et al. 2012) find that, for these DOGs, the SEDs at rest-frame mid- and far-IR wavelengths are similar to those of low redshift galaxies with IR luminosities dominated by AGN emission, such as Markarian 231. Only 2 (of 59; 3%) DOGs, and 8 (of 253; 3%) control galaxies, have SEDs that increase (in νS_ν) from observed-frame 3.6 to $8\,\mu$m, and indeed both are among the DOGs with the highest L_{IR} (at 4.8×10^{12} and 9.5×10^{12} L$_\odot$). Two galaxies are not enough to allow us to rule out the possibility that DOGs with $L_{IR} > 10^{13}$ L$_\odot$ differ in their 100 or 250 to $24\,\mu$m flux density ratios from control galaxies with similar luminosities.

Most galaxies in our sample have 10^{12} L$_\odot$ $< L_{IR} < 10^{13}$ L$_\odot$. Whether their IR luminosities are dominated by emission from AGN or newly formed stars is not clear. Fiore et al. (2008) and Treister et al. (2009) find that the average DOG in this L_{IR} range has an X-ray spectrum with a power-law index they interpret as indicative of heavily obscured AGN emission. An obscured AGN would presumably contribute to the IR luminosity as well. Pope et al. (2008) find the same average X-ray index for a similar sample of DOGs, but also find PAH emission in the mid-infrared spectra of the DOGs; they conclude that heavily obscured AGN emission cannot coexist with PAH emission. Pope et al. (2008) attribute the X-ray emission of the DOGs to X-ray bina-

ries rather than AGN. In our sample, 5 (of 61; 8%) DOGs and 31 (of 268; 12%) control galaxies have detected X-ray emission (Alexander et al. 2003). For galaxies with $L_{IR} < 10^{13}$ L$_\odot$, we do not find any evidence that AGN emission at rest-frame mid-IR wavelengths is more or less common in DOGs than in the control galaxies: the fractions of DOGs and control galaxies with increasing SEDs between observed-frame 3.6 μm and 8 μm are similar, as are the fractions with detected X-ray emission. No matter what powers their IR luminosities, DOGs in this L_{IR} range are abnormally UV faint, and are probably the most obscured galaxies.

We have shown that the brightness of the emergent UV emission in $z \sim 2$ dusty galaxies can vary considerably from galaxy to galaxy, even though the emergent UV emission is only a fraction of the IR emission. In a dusty galaxy at either low or high redshift, most of the intrinsic UV emission from newly formed stars and/or AGN is absorbed by dust grains, which emit at IR wavelengths. We now ask: "Are the UV-emitting regions that we see from a DOG or a control galaxy spatially coincident with the IR-emitting regions?" If yes, the variation in emergent UV emission is due to UV obscuration. If no, the emergent UV emission may come from stars in a "normal" galactic disk, whereas the newly formed stars ultimately responsible for the IR emission are completely obscured, perhaps in a compact, nuclear star-forming region. In this scenario, the variation in the rest-frame optical to UV flux density ratios might be due as much to differences in the stellar populations from galaxy to galaxy as to differences in obscuration (Charmandaris et al. 2004).

We cannot yet efficiently spatially resolve the IR-emitting regions for large samples of high redshift dusty galaxies. Two pieces of circumstantial evidence support the statement that the UV- and IR-emitting regions in these dusty galaxies are spatially coincident: 1) a minority of DOGs and control galaxies deviate from the median specific SFR for galaxies at $z \sim 2$; and 2) DOGs and control galaxies define a continuous relation between their median IR to UV luminosity ratios and median UV continuum power-law indices.

The specific star formation rate of a galaxy is the ratio of its SFR to its stellar mass. Most star-forming galaxies at the same redshift fall on a tight relation between SFR and stellar mass; this relation is referred to as the "main sequence" (Noeske et al. 2007; Elbaz et al. 2007; Daddi et al. 2007; Pannella et al. 2009a). Elbaz et al. (2011) find that SFR and stellar mass are directly proportional at all redshifts, and present the evolution of the median specific SFR for galaxies at $0 < z < 2.5$. Elbaz et al. (2011) also isolate the minority of galaxies with specific SFRs much higher than the median values ("starbursts"). Here, we define starbursts as galaxies with specific SFRs higher than 3 times the median value at their redshift. A minority of DOGs (5 of 25; 20%) and control galaxies (18 of 72; 25%) are starbursts (Fig. 8). Elbaz et al. (2011) find that individual low redshift starbursts have compact UV-emitting regions; the correspondence between deviation from the median specific SFR and the compact size of the UV-emitting region also holds for the average $z \sim 2$ starburst. If this correspondence holds for individual $z \sim 2$ galaxies, few DOGs and control galaxies would have concentrated UV-
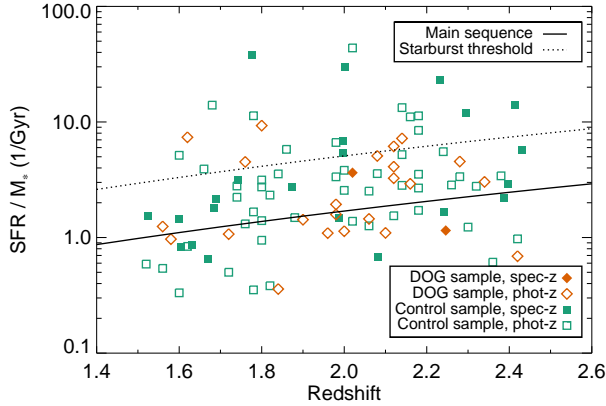
Figure 8. Specific star formation rate (SFR over stellar mass) vs. redshift for galaxies with detected $100\,\mu m$ emission. The solid line is the median specific SFR for star-forming galaxies, as a function of redshift (Elbaz et al. 2011). The dotted line is three times the median value, which we use as a threshold for identifying starbursts. 20% of DOGs and 25% of control galaxies are starbursts. DOGs deviate from the median specific SFR no more frequently than do the control galaxies.

Figure 9. L_{IR} over $0.16\,\mu m$ luminosity (IRX) vs. UV continuum power-law index (β) for galaxies with detected $100\,\mu m$ emission. We only show errors on the UV power-law indices. Filled hourglasses and circles show the median β values, in bins of IRX; the vertical bars show the range of IRX over which the β values are binned. The "average LBG" black asterisk is from Reddy et al. (2012), and shows a mean and its dispersion. The solid line is the local IRX-β relation from Overzier et al. (2011).

emitting regions. These regions in the typical DOG or control galaxy would be more widely distributed, and it would be less plausible that the UV-emitting regions occupy parts of the galaxy not occupied by IR-emitting regions. That radio-emitting regions in high redshift galaxies are widely distributed indirectly supports this idea (Rujopakarn et al. 2011).

For starburst galaxies at low redshift, Meurer et al. (1999, and more recently Overzier et al. 2011) find a relation between the ratio of IR to UV luminosities (denoted IRX) and the power-law index of the SED in the UV (denoted β). (Meurer et al. 1999 refer to low redshift galaxies with bright UV-emitting regions as "starbursts"; the term does not necessarily refer to galaxies that deviate from the main sequence.) This relation is generally interpreted to mean that the IR emission originates as UV emission from newly formed stars, which is partially absorbed by dust. The dependence between the emergent UV emission, the dust emission in the IR, and β, in the local IRX-β relation is consistent with the dependence of dust absorption on β in the Calzetti et al. (1994, 2000) dust attenuation law. In other words, we think that galaxies that lie on this relation are thought to have spatially coincident UV- and IR-emitting regions. Reddy et al. (2010, 2012) show that most Lyman break galaxies (LBG) at $z \sim 2$ lie on the local IRX-β relation. However, both $z \sim 2$ LBGs and the low redshift starbursts in Meurer et al. (1999) are much less dusty than DOGs. Some sub-classes of dusty galaxies deviate from the local relation, perhaps because their IR emission is unrelated to their emergent UV emission (Goldader et al. 2002; Chapman et al. 2005; Papovich et al. 2006; Bauer et al. 2011).

Fig. 9 shows the local IRX-β relation from Overzier et al. (2011) and the relevant quantities for the $z \sim 2$ dusty galaxies in our samples. Individual galaxies, in both the DOG and control samples, are found on either side of the relation. Because DOGs are so faint in the UV, it is difficult to precisely determine the power-law indices of their UV SEDs; the large uncertainties
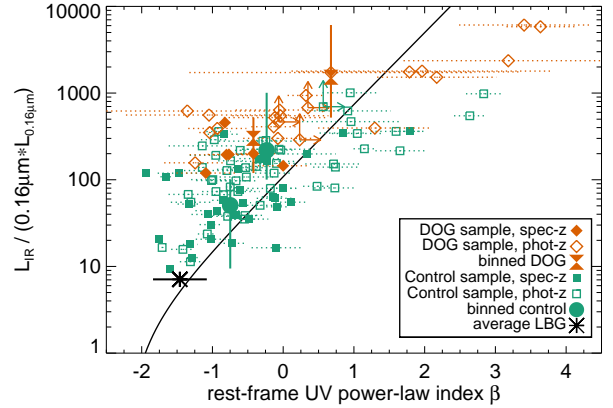
on β values preclude us from reaching firm conclusions about individual galaxies. The median β values for the DOG and control samples tend to lie to the left of the local IRX-β relation; DOGs do not appear to deviate more strongly from the relation than do control galaxies. These $z \sim 2$ dusty galaxies define their own IRX-β relation. As noted earlier, specific sub-populations of dusty galaxies deviate from the local relation, but the trend that we find between the averages for a broader $z \sim 2$ population has not been discussed. Because the median β value increases with increasing IRX, from the LBGs to the DOGs, the IR emission is not completely independent of the emergent UV emission in these galaxies. This reinforces our initial conclusion that $z \sim 2$ dusty galaxies populate a continuum of UV obscuration, and that DOGs are simply the most heavily obscured galaxies.

DOGs in the luminosity range spanned by our sample are more obscured than the control galaxies for a reason unrelated to their far-IR luminosity, because the L_{IR} distributions of the two samples are statistically indistinguishable. In galaxies with dust heated by UV emission from newly formed stars, the amount of obscuration affecting that UV emission can vary due to either: 1) differences in the degree of alignment between the spatial distributions of dust and newly formed massive stars; or 2) differences in the total dust content.

Meurer et al. (1999) derive the local IRX-β relation by assuming a uniform screen of dust in the line of sight between us and the newly formed stars (see figure 8 in Calzetti et al. 1994 for an illustration). Gordon et al. (1997) show that this assumption can be recovered when the dust is instead distributed in clumps around star-forming regions. Thus, DOGs might be more obscured than the control galaxies because DOGs have more dust clumps surrounding star-forming regions.

Variations in UV obscuration might also be caused by differences in the physical properties responsible for the shape of the sub-millimeter SED. For example, increases in the mass of cold dust can result in greater UV obscuration. Increases in the cold dust mass can also result

in increases in sub-millimeter emission. Since the sub-millimeter luminosity is usually a small fraction of the total IR luminosity, the increase in total IR luminosity due to a higher cold dust mass would not be easily measurable between 100 and $250\,\mu m$. We cannot fully test this hypothesis without sub-millimeter luminosities for galaxies in our samples. The sensitivities of current sub-millimeter facilities limit comparisons of the dust content between DOGs and control galaxies to the most luminous ($L_{IR} > 10^{13}\,L_{\odot}$) galaxies (Bussmann et al. 2009b; Magdis et al. 2011).

Currently available data do not allow us to discriminate between any hypotheses for the physical mechanisms responsible for either the differences in the degree of alignment between dust and stars or differences in the dust content. For instance, two plausible hypotheses are that: 1) galaxy inclination might be responsible for the patchiness of dust in the line-of-sight, and 2) many DOGs are merging galaxies, and some aspect of the merging process creates differences in the degree of alignment. To falsify either we require high resolution rest-frame optical images; the Cosmic Assembly Near-infrared Deep Extragalactic Legacy Survey (CANDELS) will obtain such images using HST/WFC3 in the near future (Grogin et al. 2011). We note that Kartaltepe et al. (2012) and Schawinski et al. (2012) examine rest-frame optical images of DOGs in GOODS-S and conclude that most are undisturbed disk galaxies. Furthermore, Narayanan et al. (2010) simulate isolated galaxies that meet the DOG selection criterion, so DOGs are not necessarily merging galaxies on the basis of their extreme rest-frame mid-IR to UV flux density ratios.

Finally, UV obscuration is affected by the prominence of the "dust bump" at rest-frame 2175 Å in a galaxy's attenuation curve. At $z \sim 2$, rest-frame 2175 Å is redshifted into the R-band filter. The presence of this feature in the attenuation curves of high redshift galaxies has been controversial; the bump is found, though, in the attenuation curves for several samples of galaxies at $z > 1$ (Noll et al. 2009; Buat et al. 2011, 2012). However, doubling the amplitude of the average bump leads to a reduction in the $0.65\,\mu m$ flux density by a factor of 1.3. This is not large enough to explain the spread of $S_{2.2}/S_{0.65}$ in Fig. 7.

5. CONCLUSIONS

1. We cull a sample of dust-obscured galaxies (DOGs), or galaxies with $S_{24}/S_{0.65} > 986$ that are at $1.5 < z < 2.5$, in the GOODS-N region. We use deep GOODS-$Herschel$ data to compare the emission from DOGs with that from other $z \sim 2$ galaxies with detected $24\,\mu m$ emission.

2. The DOGs in our sample span $10^{12}\,L_{\odot} \lesssim L_{IR} \lesssim 10^{13}\,L_{\odot}$. DOGs and control galaxies, with detected $100\,\mu m$ emission, have similar distributions of IR luminosities and stellar masses.

3. We compare the rest-frame far-IR and optical flux densities of DOGs with those of the control galaxies. DOGs have extreme ratios of $S_{24}/S_{0.65}$ not because they are abnormally bright at rest-frame $8\,\mu m$ for their far-IR flux densities, but because they are abnormally faint in the rest-frame UV.

4. DOGs and the control galaxies scatter around the median specific SFR established by $z \sim 2$ galaxies falling on the "main sequence"; 20% of DOGs have specific SFRs greater than 3 times the median value, and are thus starbursts. If UV-emitting regions in high-redshift starbursts are distributed as they are in low-redshift starbursts, few DOGs have compact UV-emitting regions.

5. For both the DOG and control samples, the median rest-frame UV continuum power-law index (β) at a given IR to UV luminosity ratio (IRX) is lower than the index predicted by the local IRX-β relation. DOGs do not appear to deviate more from this relation than do the control galaxies. Over more than a factor of 100 in IRX, the median β value for these galaxies systematically increases with increasing IRX.

6. These pieces of evidence suggest that, for most of these galaxies, the UV- and IR-emitting regions are spatially coincident. Thus, the range in rest-frame mid-IR to UV flux density ratios spanned by dusty galaxies at $z \sim 2$ is due to differing amounts of UV obscuration. DOGs are the most heavily obscured galaxies.

7. Differences in the amount of obscuration between DOGs and other dusty galaxies at $z \sim 2$ can be due to: 1) differences in the degree of alignment between the spatial distributions of dust and massive stars, or 2) differences in the total dust content.

Our samples do not have many galaxies with $L_{IR} \gtrsim 10^{13}\,L_{\odot}$. In DOGs with these IR luminosities, where AGN emission may be the dominant source of dust heating, our conclusions about obscuration may not be valid.

Further information about the nature of obscuration in these galaxies can come from measurements that spatially resolve UV- and IR-emitting regions. For instance, the Hα to Hβ line ratio varies with the amount of dust absorption, so its variation across a galaxy traces the spatial dust distribution. Brand et al. (2007) measure the galaxy-wide Balmer decrement for several very luminous DOGs (those most likely to have IR luminosities dominated by AGN emission); Melbourne et al. (2011) present spatially resolved Hα maps, but Hβ is outside their spectral window. HST can resolve the rest-frame UV and optical emission from these galaxies (Bussmann et al. 2009a, 2011; Kartaltepe et al. 2012), and ALMA will resolve the IR emission and allow us to measure sub-millimeter luminosities we need to determine cold dust mass. Studies using such data will clearly establish the degree to which the spatial distributions of dust and massive stars align.

REFERENCES

Alexander, D. M., Bauer, F. E., Brandt, W. N., et al. 2003, AJ, 126, 539

Barger, A. J., Cowie, L. L., & Wang, W.-H. 2008, ApJ, 689, 687

Bauer, A. E., Conselice, C. J., Pérez-González, P. G., et al. 2011, MNRAS, 417, 289

Bertin, E., & Arnouts, S. 1996, A&AS, 117, 393

Brand, K., Dey, A., Desai, V., et al. 2007, ApJ, 663, 204

Buat, V., Giovannoli, E., Heinis, S., et al. 2011, A&A, 533, A93

Buat, V., Noll, S., Burgarella, D., et al. 2012, arXiv:1207.3528

Bussmann, R. S., Dey, A., Lotz, J., et al. 2009, ApJ, 693, 750

Bussmann, R. S., et al. 2009, ApJ, 705, 184

Bussmann, R. S., Dey, A., Lotz, J., et al. 2011, ApJ, 733, 21

Calzetti, D., Kinney, A. L., & Storchi-Bergmann, T. 1994, ApJ, 429, 582

Calzetti, D., et al., 2000, ApJ, 533, 682

Capak, P., et al. 2004, AJ, 127, 180

Chapman, S., et al. 2005, ApJ, 622, 772

Charmandaris, V., Le Floc'h, E., & Mirabel, I. F. 2004, ApJ, 600, L15

Chary, R., & Elbaz, D. 2001, ApJ, 556, 562

Daddi et al. 2007, ApJ, 670, 173

Dey, A., et al. 2008, ApJ, 677, 943

Drory, N., Bender, R., & Hopp, U. 2004, ApJ, 616, L103

Elbaz et al. 2007, A&A, 468, 33

Elbaz, D., Hwang, H. S., Magnelli, B., et al. 2010, A&A, 518, L29

Elbaz, D., Dickinson, M., Hwang, H. S., et al. 2011, A&A, 533, A119

Elston, R., Rieke, G. H., & Rieke, M. J. 1988, ApJ, 331, L77

Fiore, F., et al. 2008, ApJ, 672, 94

Goldader, J. D., et al. 2002, ApJ, 568, 651

Gordon, K. D., Calzetti, D., & Witt, A. N. 1997, ApJ, 487, 625

Graham, J. R., & Dey, A. 1996, ApJ, 471, 720

Griffin, M. J., Abergel, A., Abreu, A., et al. 2010, A&A, 518, L3

Grogin, N. A., Kocevski, D. D., Faber, S. M., et al. 2011, ApJS, 197, 35

Hwang, H. S., Elbaz, D., Lee, J. C., et al. 2010, A&A, 522, A33

Hu, E. M., & Ridgway, S. E. 1994, AJ, 107, 1303

Kartaltepe, J. S., Dickinson, M., Alexander, D. M., et al. 2012, ApJ, 757, 23

Kennicutt, R., 1999, ARA&A, 36, 189

Lin, L., Dickinson, M., Jian, H.-Y., et al. 2012, ApJ, 756, 71

Magdis, G. E., Daddi, E., Elbaz, D., et al. 2011, ApJ, 740, L15

Magnelli, B., Elbaz, D., Chary, R. R., Dickinson, M., Le Borgne, D., Frayer, D. T., & Willmer, C. N. A. 2011, A&A, 528, A35

McCarthy, P. J. 2004, ARA&A, 42, 477

Melbourne, J., et al. 2011, AJ, 141, 141

Melbourne, J., Soifer, B. T., Desai, V., et al. 2012, AJ, 143, 125

Meurer, G. R., Heckman, T. M., & Calzetti, D. 1999, ApJ, 521, 64

Mullaney, J. R., et al. 2012, MNRAS, 419, 95

Narayanan, D., Dey, A., Hayward, C. C., et al. 2010, MNRAS, 407, 1701

Noeske et al. 2007, ApJ, 660, L43

Noll, S., et al. 2009, A&A, 499, 69

Overzier, R. A., Heckman, T. M., Wang, J., et al. 2011, ApJ, 726, L7

Pannella, M., Carilli, C. L., Daddi, E., et al. 2009, ApJ, 698, L116

Pannella, M., Gabasch, A., Goranova, Y., et al. 2009, ApJ, 701, 787

Papovich, C., Moustakas, L. A., Dickinson, M., et al. 2006, ApJ, 640, 92

Pilbratt, G. L., Riedinger, J. R., Passvogel, T., et al. 2010, A&A, 518, L1

Poglitsch, A., Waelkens, C., Geis, N., et al. 2010, A&A, 518, L2

Pope, A., et al. 2008, ApJ, 689, 127

Reddy, N. A., Erb, D. K., Pettini, M., Steidel, C. C., & Shapley, A. E. 2010, ApJ, 712, 1070

Reddy, N., Dickinson, M., Elbaz, D., et al. 2012, ApJ, 744, 154

Riguccini, L., Le Floc'h, E., Ilbert, O., et al. 2011, A&A, 534, A81

Rujopakarn, W., Rieke, G. H., Eisenstein, D. J., & Juneau, S. 2011, ApJ, 726, 93

Salpeter, E. E., 1955, ApJ, 121, 161

Schawinski, K., Simmons, B. D., Urry, C. M., Treister, E., & Glikman, E. 2012, MNRAS, L488

Tran, Q. D., Lutz, D., Genzel, R., et al. 2001, ApJ, 552, 527

Treister, E., Cardamone, C. N., Schawinski, K., et al. 2009, ApJ, 706, 535

Tyler, K. D., et al. 2009, ApJ, 691, 1846

Wang, W.-H., Cowie, L. L., Barger, A. J., Keenan, R. C., & Ting, H.-C. 2010, ApJS, 187, 251